

## KINK AND LONGITUDINAL OSCILLATIONS IN THE MAGNETIC NETWORK ON THE SUN: NONLINEAR EFFECTS AND MODE TRANSFORMATION

S. S. HASAN

Indian Institute of Astrophysics, Bangalore-560034, India

W. KALKOFEN AND A. A. VAN BALLEGOIJEN

Harvard-Smithsonian Center for Astrophysics, 60 Garden Street, Cambridge, MA 02138

AND

P. ÜLMSCHNEIDER

Institute für Theoretische Astrophysik, Tiergartenstrasse 15, 69012 Heidelberg, Germany

Received 2002 April 2; accepted 2002 November 13

### ABSTRACT

We examine the propagation of kink and longitudinal waves in the solar magnetic network. Previously, we investigated the excitation of network oscillations in vertical magnetic flux tubes through buffeting by granules and found that footpoint motions of the tubes can generate sufficient wave energy for chromospheric heating. We assumed that the kink and longitudinal waves are decoupled and linear. We overcome these limitations by treating the nonlinear MHD equations for coupled kink and longitudinal waves in a thin flux tube. For the parameters we have chosen, the thin tube approximation is valid up to the layers of formation of the emission features in the H and K lines of Ca II, at a height of about 1 Mm. By solving the nonlinear, time-dependent MHD equations we are able to study the onset of wave coupling, which occurs when the Mach number of the kink waves is of the order of 0.3. We also investigate the transfer of energy from the kink to the longitudinal waves, which is important for the dissipation of the wave energy in shocks. We find that kink waves excited by footpoint motions of a flux tube generate longitudinal modes by mode coupling. For subsonic velocities, the amplitude of a longitudinal wave increases as the square of the amplitude of the transverse wave, and for amplitudes near Mach number unity, the coupling saturates and becomes linear when the energy is nearly evenly divided between the two modes.

*Subject headings:* MHD — Sun: magnetic fields — Sun: oscillations

### 1. INTRODUCTION

It is well known that magnetic fields play an important role in the dynamics and heating of the solar chromosphere. In the quiet chromosphere we distinguish the magnetic network on the boundary of supergranulation cells, where strong magnetic fields are organized in magnetic flux tubes, and internetwork regions in the cell interior, where magnetic fields are weak and dynamically unimportant.

Ground-based observations of the Ca II H and K lines, which are formed in the low chromosphere, show similar emission from network and internetwork regions. While instantaneous grains from the internetwork may outshine network bright points (see Fig. 1 of Lites, Rutten, & Kalkofen 1993), the long-time average intensity shows total calcium emission from the network to be more important (see Fig. 1 of von Uexküll & Kneer 1995). In addition to having higher average intensity, network bright points also have longer periods, typically about minutes (Lites et al. 1993; Curdt & Heinzel 1998), and the time variation of their intensity profile is much less peaked. Note that recent observations by McAteer et al. (2002) suggest the presence of multiple peaks in the power spectrum, with periods in the 4–15 minute range.

Space-based observations of UV spectral lines and continua provide important constraints on the structure and dynamics of the chromosphere and chromosphere-corona transition region. Observations with SUMER have shown that the UV lines are always in emission, consistent with semiempirical models in which the temperature in the

chromosphere increases with height at all times (Vernazza, Avrett, & Loeser 1981). Internetwork regions show large-scale coherent oscillations with length scales of 3–7 Mm and periods between 120 and 200 s in spectral lines of neutral and singly ionized species, and sometimes also in lines from higher ionization states (Carlsson, Judge, & Wilhelm 1997; Wikstøl et al. 2000; McIntosh et al. 2001). These oscillations, which have also been seen with *TRACE* (Rutten, de Pontieu, & Lites 1999; Judge, Tarbell, & Wilhelm 2001; Krijger et al. 2001), suggest that there are upward-propagating waves in the nonmagnetic chromosphere that sometimes drive oscillations in the overlying transition region. Network regions are brighter than internetwork regions and show strong oscillatory power only at lower frequencies (Judge, Carlsson, & Wilhelm 1997). Transition region lines from the network show persistent redshifts, and the line widths indicate the presence of subsonic, unresolved nonthermal Doppler motions of several kilometers per second (Dere & Mason 1993; Peter 2001). Furthermore, there is a strong correlation between high intensity and redshift (Hansteen, Betta, & Carlsson 2000). Curdt & Heinzel (1998) found evidence for upward propagating waves within the network (also see Heinzel & Curdt 1999). However, they were unable to identify the wave modes responsible for these oscillations.

The phenomena in the magnetic network and in the non-magnetic cell interior show superficial similarity. Yet while the physics of the cell interior is fairly well understood (although controversial), the same cannot be claimed for the network. It is therefore instructive to compare our

understanding of the phenomena in the two media. The steady radiative emission of the nonmagnetic chromosphere is well described by the empirical models of Vernazza et al. (1981) and Fontenla, Avrett, & Loeser (1993). The models imply that the nonmagnetic chromosphere is continually heated, perhaps by ubiquitous weak shocks. In addition, there are stronger, more intermittent shocks that are responsible for the internetwork grains seen in the Ca II H and K lines (Carlsson & Stein 1995, 1997). According to the empirical models by Vernazza et al. (1981) and Fontenla et al. (1993), the temperature structure of the magnetic chromosphere is very similar to that of the nonmagnetic chromosphere, suggesting that the heating mechanisms in the two media may be similar. However, the statistics of H and K line asymmetries and the periods of oscillations in the magnetic network are significantly different from those of calcium grains in the cell interior (Grossmann-Doerth, Kneer, & von Uexküll 1974). These differences may find an explanation in the wave modes and the mechanisms of excitation of oscillations in the two media.

G-band (4305 Å) observations have revealed the presence of bright points in the magnetic network, which are in a highly dynamical state due to the buffeting action of granules (e.g., Muller 1985; Muller et al. 1994; van Ballegoijen et al. 1998). The magnetic field in the network can be idealized in terms of isolated vertical flux tubes in the photosphere that fan out with height. It is well known that flux tubes support a variety of wave modes: the sausage or longitudinal mode, the kink or transverse mode, and the torsional Alfvén mode (Spruit 1982; Roberts & Ulmschneider 1997). The earliest studies on MHD wave excitation were based on extensions of the Lighthill (1952) mechanism (Kulsrud 1955; Osterbrock 1961; Stein 1967, 1968; Musielak & Rosner 1987; Collins 1989, 1992). More recently, Musielak, Rosner, & Ulmschneider (1989), Musielak et al. (1995), Huang, Musielak & Ulmschneider (1995), and Ulmschneider & Musielak (1998) examined the generation of longitudinal and transverse waves in a flux tube by turbulent motions in the convection zone. An alternative scenario motivated by observational considerations suggests that transverse waves can be generated through the impulse imparted by granules to magnetic flux tubes (Choudhuri, Auffret, & Priest 1993; Choudhuri, Dikpati, & Banerjee 1993; Kalkofen 1997; Steiner et al. 1998). These investigations suggested that the kink wave energy flux could be important for coronal heating.

Hasan & Kalkofen (1999, hereafter Paper I) investigated the impulsive excitation of transverse and longitudinal waves by granular motions in the magnetic network. The response of a flux tube to a single granular impact is the same for both transverse and longitudinal waves: the buffeting action excites a pulse that propagates along the flux tube with the kink or longitudinal tube speed, respectively. For strong magnetic fields, most of the energy goes into transverse waves, and only a much smaller fraction into longitudinal waves. After the passage of the pulse, the atmosphere gradually relaxes to a state in which it oscillates at the cutoff period of the mode. These results show that the first pulse carries most of the energy and after this pulse has passed the atmosphere oscillates in phase without energy transport. The period observed in the magnetic network is interpreted as the cutoff period of transverse waves, which leads naturally to an oscillation at this period (typically in the 7 minute range) as proposed by Kalkofen (1997). In reality, we expect

the excitation of waves in a tube to occur not as a single impact but continually, due to the highly turbulent and stochastic motion of granules.

Hasan, Kalkofen, & van Ballegoijen (2000) modeled the excitation of waves in the network due to the observed motions of G-band bright points, which were taken as a proxy for footpoint motions of flux tubes. For a typical magnetic element in the network they predicted that the injection of energy into the chromosphere takes place in brief and intermittent bursts, lasting typically 30 s, separated by long periods with low energy flux; this implies a high intermittency in chromospheric emission, which is incompatible with observations. They concluded that there must be other high-frequency motions (periods 5–50 s) which cannot be detected as proper motions of G-band bright points. Adding such high-frequency motions to the simulations, they obtained much better agreement with the persistent emission observed from the magnetic network. They speculated that the high-frequency motions could be due to turbulence in intergranular lanes, but some aspects of this model need further investigation and will be considered in a future study.

The above-mentioned work was based on a linear approximation in which the longitudinal and transverse waves are decoupled. However, the velocity amplitude  $v(z)$  for the two modes increases with height  $z$  (for a thin flux tube in an isothermal atmosphere, as  $v \propto \exp(z/4H)$ , where  $H$  is the pressure scale height), due to which the motions become supersonic higher up in the atmosphere. At such heights, nonlinear effects become important, leading to coupling between the transverse and longitudinal modes. Some progress on this question has been made using the nonlinear equations for a thin flux tube (Ulmschneider, Zähringer, & Musielak 1991; Huang, Musielak, & Ulmschneider 1995). This work has been extended to include a treatment of kink and longitudinal shocks (Zhugzhda, Bromm, & Ulmschneider 1995). These investigations have concentrated primarily on wave propagation in the photosphere and in the lower chromosphere. The motivation for the present work is to examine in detail the onset of nonlinear effects along with their implications in a vertical flux tube. These produce significant mode coupling, leading to a transfer of energy between the modes, which is likely to have important consequences for the dynamics and energy transport in the solar network.

The main aim of this study is to extend the calculations of Paper I and include the coupling of transverse and longitudinal modes through nonlinear effects. We use the thin flux tube approximation in an isothermal atmosphere, which has the advantage that the linear solutions can be determined analytically and compared with the nonlinear ones. This enables us to delineate the regions of the atmosphere where nonlinear effects become important. The emphasis in this investigation is to understand the nature of mode coupling and its consequences. In future work we hope to extend the present calculations to more general conditions.

The organization of this paper is as follows: in § 2 we present a two-dimensional model of a magnetic flux tube to justify the use of the thin tube approximation up to heights in the middle chromosphere. Section 3 discusses the excitation of MHD waves by footpoint motions in a “thin” flux tube. In § 4, we present the results of model calculations to focus on nonlinear effects and mode coupling. The broad implications of our investigation along with its main conclusions are presented in § 5.

## 2. TWO-DIMENSIONAL FLUX TUBE MODEL

Let us consider a flux tube extending vertically through the photosphere and chromosphere of the Sun. We model its structure in cylindrical geometry assuming axial symmetry. The flux tube is contained within a cylinder of radius  $R_0$ , which represents the space available to the flux tube in the solar atmosphere. The total magnetic flux of the tube is given by  $\Phi_0$ . The flux tube radius  $R(z)$  is a function of height  $z$  above the level where the optical depth  $\tau_{5000} = 1$  in the nonmagnetic photosphere. Below some height  $z_c$ , the radius  $R(z)$  is less than  $R_0$ , and the tube is embedded in a field-free medium that fills the remainder of the cylindrical space. At these heights there is a sharp boundary between the flux tube and its local surroundings. The flux tube radius  $R(z)$  increases with height, and at  $z = z_c$  (the “canopy” height) the boundary of the flux tube reaches the wall of the cylinder,  $R(z_c) = R_0$ . Above this height the magnetic field is vertical along the cylinder wall. This model simulates the effect of neighboring flux tubes, which prevent the further expansion of the tube with height (we assume that neighboring flux tubes have the same magnetic polarity). Therefore, the quantity  $2R_0$  can be interpreted as the distance between neighboring flux tubes. In this paper we consider a model with  $\Phi_0 = 5 \times 10^{16}$  Mx,  $R_0 = 1000$  km, and  $z_c = 1200$  km. The cylinder extends from  $z_b = -300$  km below the photosphere to  $z_t = 2500$  km in the corona.

Appendix A describes how the magnetic structure of the flux tube is computed. Briefly, the interior of the flux tube is assumed to be in magnetostatic equilibrium and the gas pressures inside and outside the flux tube are based on the semiempirical models of Vernazza, Avrett, & Loeser (1981). The magnetic field strength at  $z = 0$  in the photosphere is about 1590 G, and the flux tube radius at that height is 33 km. Figure 1 shows the result of the numerical computation. The solid lines show the magnetic field lines, including the field line that forms the boundary between the flux tube and the external medium. The dashed line shows the location of the boundary as computed using the thin flux tube approximation ( $R \propto p_{\text{ext}}^{-0.25}$ ). For  $z < 1000$  km the tube radii calculated from the two-dimensional model and from the thin tube approximation are nearly identical. At  $z = 1000$  km the difference is only 9%, even though the flux tube radius at this height (about 354 km) is greater than the local pressure scale height (about 150 km). At larger heights, the thin tube approximation fails rapidly owing to the expansion of the flux tube near the “canopy” height of 1200 km.

Another method for comparing the two-dimensional and thin tube models is to consider the radial variation of magnetic field strength across the tube. The thin tube approximation assumes that the field strength is constant with radius. The inset in Figure 1 shows the variation of field strength at heights of 800 and 1000 km in the two-dimensional model. We find that the field strength decreases from the axis of the tube to the boundary by about 9% and 27%, respectively. We conclude that the thin tube approximation is valid up to a height of about 1000 km.

## 3. WAVE EXCITATION DUE TO FOOTPOINT MOTION

In this section we study wave propagation in a tube over a height range where the thin flux tube approximation is valid. We may assume that the atmosphere is isothermal since

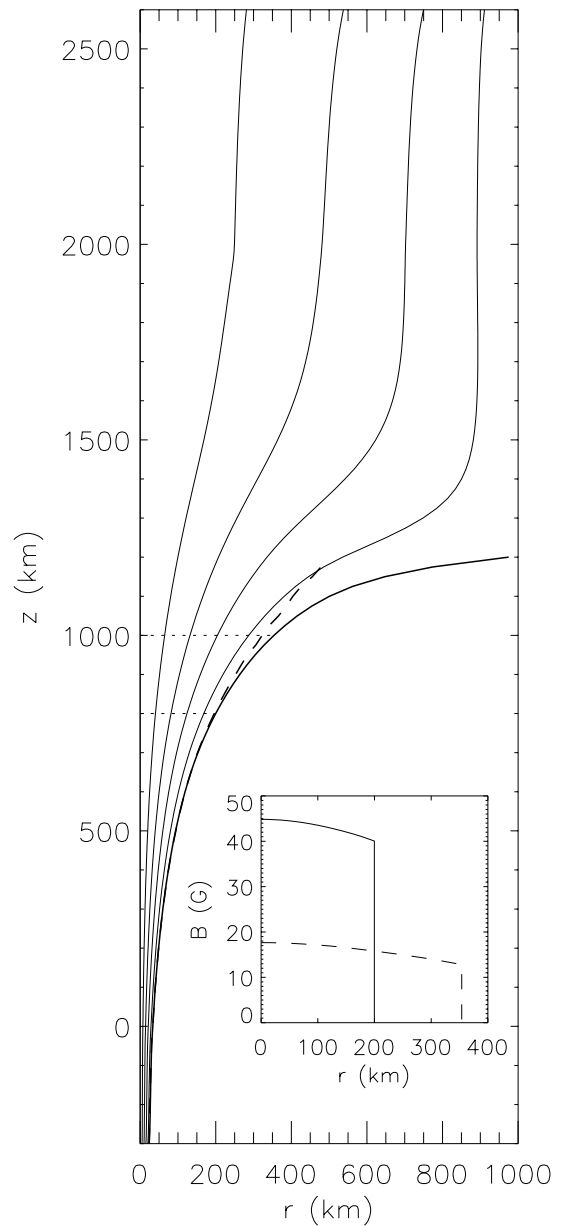


FIG. 1.—Model of a thin magnetic flux tube on the quiet Sun (magnetic flux  $\Phi_0 = 5 \times 10^{16}$  Mx). The model has cylindrical symmetry. The flux tube is embedded in a field-free region and is in pressure balance with its surroundings. The solid lines show selected magnetic field lines that expand with height in the solar atmosphere. The dashed line shows the flux tube boundary for the thin tube approximation. The inset shows the magnetic field strength as a function of radius at  $z = 800$  km (solid curve) and  $z = 1000$  km (dashed curve).

our focus is on the dynamics, which is insensitive to the temperature structure.

### 3.1. Initial Flux Tube Model

We assume that the flux tube is “thin” and initially in hydrostatic equilibrium and isothermal, with the same temperature as the external medium, and consider a tube with a radius of 40 km and a field strength of  $B = 1700$  G at  $z = 0$ , corresponding to a plasma  $\beta$  of 0.18 (which remains constant with height). We also assume that the temperature

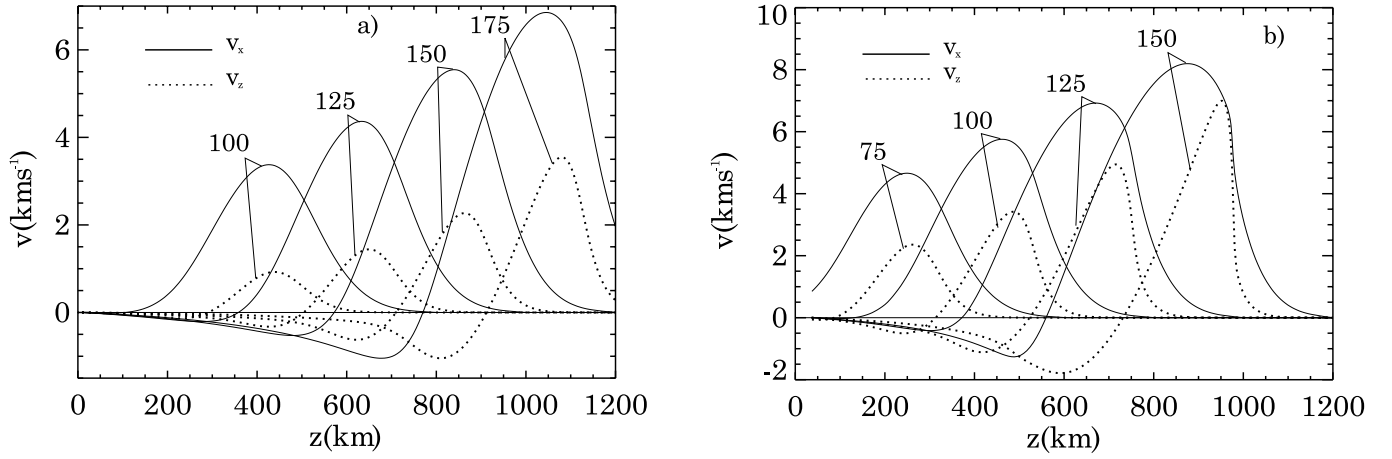


FIG. 2.—Variation of the transverse  $v_x$  (solid lines) and the longitudinal  $v_z$  (dashed lines) components of the velocity as functions of height  $z$  at various epochs for (a)  $v_0 = 2.0 \text{ km s}^{-1}$  and (b)  $v_0 = 4.0 \text{ km s}^{-1}$ . The numbers beside the curves denote the time (in seconds).

is  $T = 6650 \text{ K}$  (corresponding to a scale height  $H = 155 \text{ km}$ ). The radius of the tube increases with  $z$  as  $\exp(z/4H)$ .

### 3.2. Method of Solution

The basic equations for adiabatic longitudinal-transverse MHD waves in a thin flux tube consist of a set of coupled differential equations (see Ulmschneider et al. 1991 for details) which are solved numerically using the method of characteristics. In the present work we adopt this method, modified to include shocks, based on the treatment of Zhugzhda et al. (1995). The computational domain in the vertical direction has an equidistant grid of size  $5 \text{ km}$ . The Courant condition is used to select the time step to advance the equations in time.

### 3.3. Boundary Conditions

At the lower boundary, taken at  $z = 0$ , we assume that the flux tube has a transverse motion which consists of a single impulse with a velocity of the form:

$$v_x(0, t) = v_0 e^{-[(t-t_0)/\tau]^2}, \quad (1)$$

where  $v_0$  is the specified velocity amplitude,  $t_0$  denotes the time when the motions have maximum amplitude, and  $\tau$  is the time constant of the impulse. The longitudinal component of the velocity at the base is assumed to be zero. In the present calculations we take  $t_0 = 50 \text{ s}$  and  $\tau = 20 \text{ s}$ .

At the upper boundary of the computational domain (at  $z = 1500 \text{ km}$ ) we use transmitting boundary conditions, following Ulmschneider et al. (1977), and assume that the velocity amplitude remains constant along the outward propagating characteristics. The characteristic equations are used to self-consistently determine physical quantities at the boundary.

## 4. RESULTS

The initial equilibrium model is perturbed with a transverse motion at  $z = 0$  in the form of an impulse with a velocity given by equation (1). This impulse generates a transverse wave that propagates upward with the kink wave

speed  $c_k$ , which is about  $7.9 \text{ km s}^{-1}$  for the equilibrium model. The resulting motion in the tube as a function of height and time follows from the time-dependent MHD equations for a thin flux tube.

Figures 2a and 2b show the variation of the transverse  $v_x$  (solid lines) and longitudinal  $v_z$  (dashed lines) components of the velocity as a function of height  $z$  at various epochs of time  $t$  for  $v_0 = 2.0 \text{ km s}^{-1}$  and  $v_0 = 4.0 \text{ km s}^{-1}$ , respectively. The numbers beside the curves denote the time  $t$  (in seconds). We find that low in the atmosphere, where the transverse velocity amplitude is small (compared to the kink wave speed  $c_k$ ), the longitudinal component of the velocity is negligible. As the initial pulse propagates upward, the transverse velocity amplitude increases. Due to nonlinear effects, beginning when the Mach number  $M = v_x/c_k$  is as low as 0.3, longitudinal motions are generated. The efficiency of the nonlinear coupling increases with the amplitude of the transverse motions. When  $v_x \approx c_k$ , the amplitudes in the transverse and longitudinal components become comparable. The longitudinal motions, being compressive, steepen with height and eventually form shocks. The steepening is clearly visible in Figure 2b, especially at  $t = 150 \text{ s}$  in the longitudinal component. These results are reminiscent of those found by Hollweg, Jackson, & Galloway (1982), who studied the nonlinear coupling of torsional Alfvén waves and longitudinal waves in the solar atmosphere. Their results, however, did not show any wakes, which arise due to the presence of a cutoff frequency, which is absent for torsional Alfvén waves.

Let us now examine the temporal behavior of the velocity. Figure 3 shows the variation of the transverse  $v_x$  (solid lines) and longitudinal  $v_z$  (dashed lines) components of the velocity as functions of time  $t$  at  $z = 1000 \text{ km}$  for  $v_0 = 0.5 \text{ km s}^{-1}$ . The vertical scale on the right corresponds to  $v_z$ . The first maxima in the velocities denote the arrival of the transverse and longitudinal components of the impulse, which travel at approximately the same speed (since  $c_k \approx c_T$ ).

After the passage of the primary pulses, which eventually propagate out through the top boundary, the transverse and longitudinal components oscillate with different periods. At this stage, since the velocity amplitudes are small, the two modes essentially decouple. We find that in the

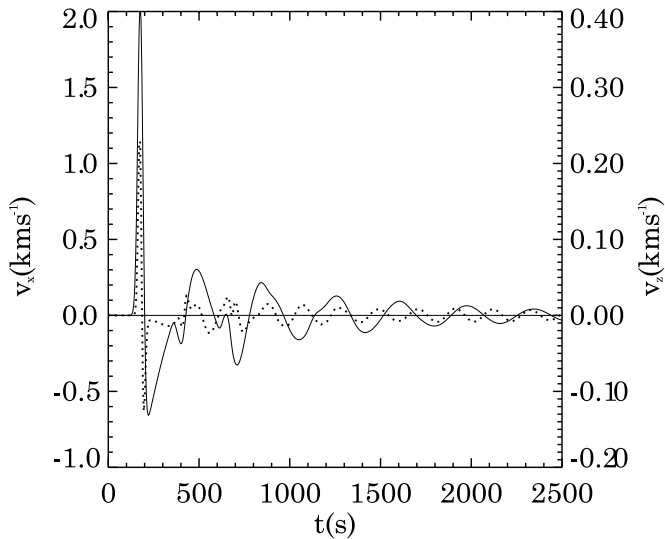


FIG. 3.—Variation of the transverse  $v_x$  (solid lines) and the longitudinal  $v_z$  (dashed lines), components of the velocity as functions of time  $t$  at  $z = 1000$  km for  $v_0 = 0.5$  km s $^{-1}$ .

asymptotic time limit, the periods of the two modes closely match their cutoff periods, which are about 490 and 230 s for kink and longitudinal waves, respectively. This result is in agreement with the linear analysis of Paper I.

We now focus on the coupling between the two modes which, as stated earlier, arises solely due to nonlinear effects. Figure 4 shows the variation of the longitudinal wave amplitude  $v_z$  as a function of the transverse wave amplitude  $v_x$  at different heights in a flux tube for  $v_0 = 2.0$  km s $^{-1}$ . At each height, we use the maximum value of the amplitude in the two components associated with the transverse and longitudinal pulses. At low values of  $v_x$ , there is essentially no coupling with the longitudinal mode, and hence  $v_z$  is practically zero. However, as  $v_x$  increases, nonlinear effects become

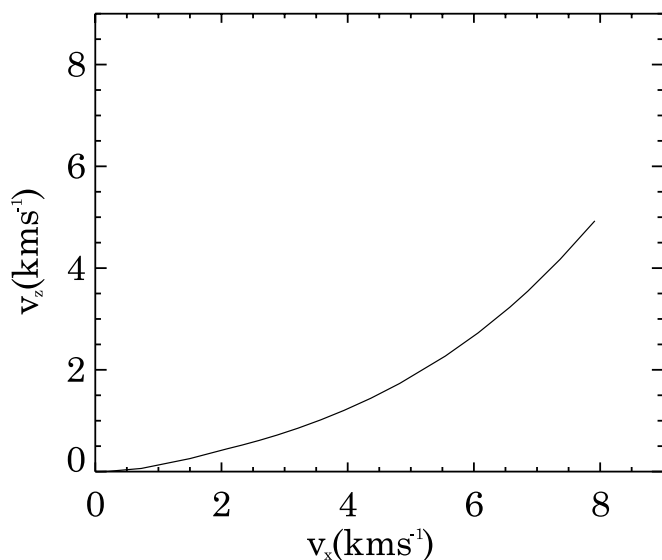


FIG. 4.—Variation of the longitudinal wave amplitude  $v_z$  as a function of the transverse wave amplitude  $v_x$  at different heights in a flux tube for  $v_0 = 2.0$  km s $^{-1}$ . At each height, we use the maximum value of the amplitude in the two components associated with each pulse.

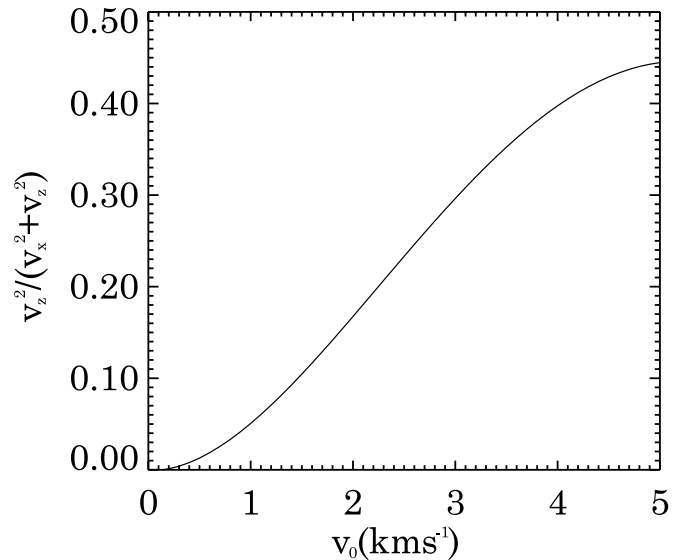


FIG. 5.—Variation of  $v_z^2/(v_x^2 + v_z^2)$  at  $z = 1000$  km as a function of  $v_0$ , the forcing transverse velocity amplitude at  $z = 0$ . We use the maximum value of the amplitude in the two components associated with the transverse and longitudinal pulses.

important and longitudinal oscillations are excited. This coupling is quadratic because these oscillations are generated by the centrifugal force that arises from the curvature of the field lines when the tube exhibits a kink oscillation. However, once  $v_x \approx c_k$ , the two modes have comparable amplitudes and  $v_z$  increases linearly with  $v_x$ .

It is instructive to consider the partitioning of energy between the two modes as the forcing amplitude of the transverse velocity at the base of the flux tube increases. Figure 5 shows the variation at  $z = 1000$  km of  $e_z = v_z^2/(v_x^2 + v_z^2)$ , the ratio of the wave energy in longitudinal motions to the total energy as a function of  $v_0$ , and the forcing transverse velocity amplitude at  $z = 0$ . Once again we use the maximum value of the velocity amplitude in the two pulses. When  $v_x \ll c_k$ , then  $e_z \sim v_z^2/v_x^2 \sim v_x^2$ , since  $v_z \sim v_x^2$  for small  $v_x$ . However, as  $v_0$  increases,  $v_x$  and  $v_z$  become comparable, and  $e_z$  saturates at a value near 0.5. The saturation value is less than 0.5 for two reasons: first, there is a nonlinear feedback from the longitudinal mode to the transverse mode, which prevents the two amplitudes from becoming the same and secondly, when the two modes have different phase speeds, the coupling becomes less efficient. In the present case, since  $c_k \approx c_T$ , we expect the nonlinear feedback to be the dominant reason.

Finally, we compare the results of the present calculation with those obtained in the linear approximation. Such a comparison helps us to delineate the regions in the atmosphere where nonlinear effects become important. As was shown in Paper I, the propagation of kink waves in a thin flux tube is governed by the Klein-Gordon equation, which can be solved exactly for an isothermal atmosphere. We consider the excitation of kink waves in an isothermal tube extending from  $z = 0$  up to  $z = 1200$  km. Furthermore, we only consider upward-propagating waves and disregard reflections. Figure 6 shows the variation of the transverse velocity  $v_x$  as a function of height  $z$  at various epochs of time  $t$  for  $v_0 = 2.0$  km s $^{-1}$ , keeping other parameters the same as before. The solid and dotted lines correspond to the linear

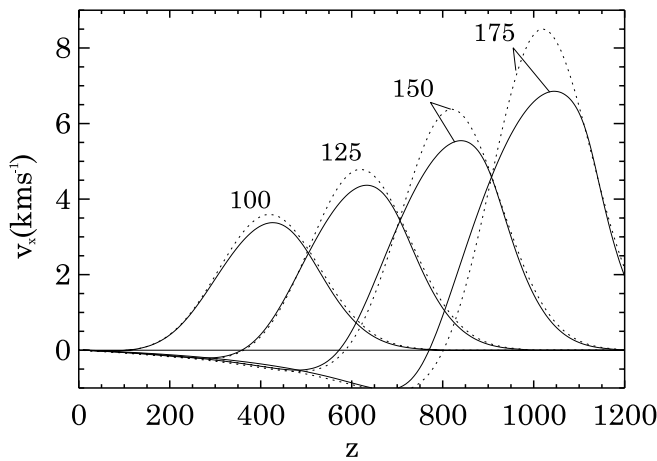


FIG. 6.—Variation of the transverse  $v_x$  velocity as a function of height  $z$  at various epochs for the linear and nonlinear cases, denoted by solid and dotted lines, respectively, assuming  $v_0 = 2.0 \text{ km s}^{-1}$  and the same parameters as before. The numbers beside the curves denote the time (in seconds).

and nonlinear cases, respectively. The numbers beside the curves denote the time  $t$  (in seconds). We find that low in the atmosphere ( $z < 300 \text{ km}$ ), where the transverse velocity amplitude is much less than the kink wave speed  $c_k$ , the linear approximation is excellent. However, as the initial pulse reaches the lower chromosphere ( $z \approx 600 \text{ km}$ ), one can clearly see the breakdown of the linear approximation. These results also provide a powerful test of our nonlinear code—the excellent agreement between the two sets of results for small to moderate velocity amplitudes demonstrates its accuracy.

## 5. DISCUSSION AND SUMMARY

The purpose of this investigation was to extend the linear calculations of Paper I to include nonlinear effects with a view to determining the nature of mode coupling between the transverse and longitudinal modes in the magnetic network. We modeled the excitation of these oscillations through impulsive footpoint motions. We found that when the transverse velocities are significantly less than the kink wave speed (the linear regime), there is essentially no excitation of longitudinal waves. However, at heights where  $v_x \sim 0.3 c_k$ , longitudinal modes begin to be excited, and when  $v_x \approx c_k$ , longitudinal wave generation becomes efficient, leading to the modes having comparable amplitudes. A comparison of the results with the exact linear solution for transverse waves enables us to locate the regions in the atmosphere where nonlinear effects are important.

We found that a transverse impulse delivered to the base of a flux tube as it travels upward generates a longitudinal pulse that eventually leads to low-amplitude waves representing decoupled longitudinal and kink waves, oscillating at their respective cutoff periods. Since the cutoff periods are well separated, this could provide an observational test of the model, which predicts that the signature of impulsive footpoint motions would be two distinct peaks in the wave power spectrum of network oscillations in the middle to upper chromosphere. We expect that the dominant peak with a period in the 6–7 minute range would correspond to the low-frequency transverse oscillations, whereas the secondary peak in the 3 minute range could be identified with

longitudinal oscillations. There is a hint that these features may be present in the observations of Lites et al. (1993), although Krijger et al. (2001) suggest a more cautious interpretation, based on a reanalysis of the same data. We should, however, note that the theoretical results presented by us are based on the assumption of the flux tube footpoints being shaken impulsively. In reality, the footpoint motion consists of several impacts (e.g., Muller et al. 1994) that probably occur stochastically, so that the power spectrum of oscillations is unlikely to show a clear separation of peaks that would occur for a single impulse.

We have examined the coupling between the two modes and find that  $v_z$  increases quadratically with  $v_x$  at low Mach number  $M$  (with respect to  $c_k$ ) and linearly with  $v_x$  for  $M \rightarrow 1$ . Transverse waves lose energy due to mode coupling. The fractional wave energy in longitudinal motions increases rapidly at first with the forcing transverse velocity,  $v_0$ , before eventually saturating at a value of about 0.45, which is close to equipartition of energy between the two modes.

We have found that large-amplitude longitudinal waves are generated in the upper photosphere from transverse waves through mode coupling; they steepen and attain shock strength in the chromosphere. Longitudinal waves, being compressive, will be rapidly dissipated once they form shocks and thereby contribute to chromospheric heating. Detailed calculations on shock heating by longitudinal waves will be taken up in a subsequent investigation, in which dissipative effects are included in the treatment. Kink or transverse waves, on the other hand, being almost incompressible, cannot easily dissipate and hence can propagate through the transition region into the corona. An estimate of the transverse energy flux entering the corona would require a more elaborate calculation than the present one.

Before concluding, let us briefly comment on some of the assumptions made in this paper and their range of validity. The theoretical treatment of MHD waves used the thin tube approximation, which simplifies the treatment considerably by allowing us to examine a complex multidimensional phenomenon in one dimension. By comparing the exact magnetostatic solution for an axisymmetric flux tube with that obtained in the thin flux tube approximation, we showed that the latter is reasonable up to height of about a 1 Mm above the photospheric base even though the radius at this height is larger than the pressure scale height. However, strictly speaking this analysis is valid for small isolated network element with a filling factor below 0.1% on the solar surface. It could be argued that such elements are rare on the Sun. For higher filling factors (say about 1%), the height up to which the thin flux tube approximation is valid would of course decrease, and a more elaborate treatment would be required to treat the merging of different tubes. Nevertheless, we believe that the essential features of our analysis on the nonlinear generation of longitudinal waves from transverse waves, the nature of the mode coupling in flux tubes and the implications for chromospheric heating are likely to hold qualitatively in the solar network, independent of the above approximation. We also reiterate that our interest in the present work is in regions of the network where the Ca K emission occurs and where the magnetic elements are still distinct.

It is interesting to comment on phenomena occurring in the higher chromosphere, particularly above the canopy, where field lines from various flux tubes merge and waves

from different tubes interact with each other. This problem is clearly outside the scope of the present investigation. However, some progress has been made in this direction by Rosenthal et al. (2002), who have carried out two-dimensional simulations to examine how the field geometry in network and internetwork regions influences wave propagation in the solar photosphere and chromosphere. Their investigation treats magneto-acoustic waves in a two-dimensional slab geometry in which the displacements lie in a plane perpendicular to the invariant direction. These waves, however, are different from the kink and sausage modes we considered, for which three-dimensional simulations would be required but have not yet been carried out. Nevertheless, the above work by Rosenthal et al. represents a useful beginning that should be followed up by more refined calculations to allow a realistic comparison with observations.

The other assumptions that were part of the model were the use of an isothermal atmosphere and the neglect of energy losses. The isothermal approximation is reasonable in the photosphere and lower chromosphere but breaks down in the upper regions. However, it was used mainly to make comparisons with our earlier linear analysis of Paper I, based on this approximation. Furthermore, the qualitative aspects of our results are unlikely to be affected by this assumption. The use of an adiabatic energy equation

is unrealistic and was made solely for mathematical reasons. We hope to incorporate these refinements in subsequent work.

In summary, we have examined in detail the coupling of transverse and longitudinal waves in a flux tube. The thin flux tube approximation was adopted to focus in a mathematically tractable manner on the physical nature of wave propagation and the onset of nonlinear effects. For small wave amplitudes we found excellent agreement between the linear and nonlinear treatments. However, when the velocity amplitudes become large (but still subsonic), nonlinear effects become important, owing to which kink waves excited by footpoint motions get converted into longitudinal waves. An important feature of the results is the presence of wakes that arise after the propagation of the pulse and are related to the existence of cutoff frequencies. After the main pulse has propagated away, the atmosphere relaxes to the linear state, with the transverse and longitudinal modes oscillating independently at their respective cutoff frequencies. We suggest that chromospheric heating occurs because of the dissipation of longitudinal waves, whereas kink waves can propagate into the corona, where they might contribute to heating.

We thank the referee for helpful comments and acknowledge support from NASA and NSF.

## APPENDIX A

### TWO-DIMENSIONAL FLUX TUBE MODEL

As described in § 2, the flux tube is embedded in a cylinder with radius  $R_0$ . The interior of the flux tube is assumed to be in magnetostatic equilibrium:

$$-\nabla p + \rho \mathbf{g} + (4\pi)^{-1}(\nabla \times \mathbf{B}) \times \mathbf{B} = 0, \quad (\text{A1})$$

where  $\mathbf{B} = [B_r(r, z), 0, B_z(r, z)]$  is the magnetic field in cylindrical coordinates,  $p$  is the gas pressure,  $\rho$  is the density, and  $\mathbf{g} = -g\hat{\mathbf{z}}$  is the acceleration due to gravity. This equation implies hydrostatic equilibrium along the field lines,  $dp/dz = -\rho g$ , where  $d/dz$  is the derivative along the field lines. Furthermore, pressure balance with the surroundings requires

$$p_{\text{int}}(z) + \frac{B_{\text{int}}^2(z)}{8\pi} = p_{\text{ext}}(z), \quad \text{for } z \leq z_c, \quad (\text{A2})$$

where  $B_{\text{int}}(z) \equiv B[R(z), z]$  is the magnetic field strength just inside the boundary of the flux tube and  $p_{\text{ext}}(z)$  is the external gas pressure. The gas pressure and density can be written as functions of  $\Phi$  and  $z$ , where  $\Phi(r, z)$  is the magnetic flux contained within a circle of radius  $r$  centered on the flux tube axis ( $0 \leq \Phi \leq \Phi_0$ ). We use the following expression for the pressure distribution inside the flux tube:

$$p(\Phi, z) = p_{\text{int}}(z) + [p_{\text{axis}}(z) - p_{\text{int}}(z)]f(\Phi)/f(0), \quad (\text{A3})$$

where  $p_{\text{axis}}(z)$  is the gas pressure on the flux tube axis,  $p_{\text{int}}(z)$  is the pressure just inside the boundary of the flux tube, and the function  $f(\Phi)$  is defined in equation (A9) below. Then the hydrostatic equilibrium condition yields

$$\rho(\Phi, z) = \rho_{\text{int}}(z) + [\rho_{\text{axis}}(z) - \rho_{\text{int}}(z)]f(\Phi)/f(0), \quad (\text{A4})$$

where  $\rho_{\text{int}}(z) \equiv -g^{-1}dp_{\text{int}}/dz$  and  $\rho_{\text{axis}}(z) \equiv -g^{-1}dp_{\text{axis}}/dz$ . The internal pressures  $p_{\text{axis}}(z)$  and  $p_{\text{int}}(z)$  are taken from the semi-empirical models C and A of Vernazza, Avrett, & Loeser (1981) and Fontenla, Avrett, & Loeser (1990, 1991, 1993). The external pressure  $p_{\text{ext}}(z)$  is taken from model MCO of Avrett (1995). The MCO model is used only below the canopy height. Since the magnetic field has a null point at  $z = z_c$  and  $r = R_0$ , the height scale of model A was shifted such that  $p_{\text{int}}(z_c) = p_{\text{ext}}(z_c)$ . The height scale of model C was shifted such that at large depth in the flux tube the gas pressure is constant across the flux tube.

It can be shown that the solution of equations (A1) and (A2) correspond to minima of the following Lagrangian:

$$W \equiv \int_{z_b}^{z_t} \int_0^{R(z)} \left[ \frac{B^2}{8\pi} - p(\Phi, z) \right] 2\pi r dr dz + \int_{z_b}^{z_c} p_{\text{ext}}(z) \pi R^2(z) dz. \quad (\text{A5})$$

The first term represents the magnetic and thermal energy of the flux tube, and the second term represents the work done against the external pressure when the flux tube radius  $R(z)$  is increased. Therefore, the magnetostatic problem can be solved using a variational method. The magnetic field is described in terms of the shapes of the field lines,  $r(\Phi, z)$ , and this function is varied until  $W$  reaches a minimum (conjugate gradient method, see Press et al. 1992). This yields the magnetic field components  $B_r(r, z)$  and  $B_z(r, z)$ , gas pressure  $p(r, z)$ , and mass density  $\rho(r, z)$ .

The magnetic field in the upper part of the cylinder is assumed to be nearly vertical, so that the total pressure  $B^2/(8\pi) + p$  is constant in horizontal planes. We assume that the vertical field at the upper boundary is given by

$$B_z(\Phi, z_t) = B_{\text{int}} \left[ 1 + \frac{1}{2} \beta \left( 1 - \frac{\Phi}{\Phi_0} \right)^2 \right]^{-1}, \quad (\text{A6})$$

where  $\beta$  is a parameter describing the radial variation of field strength. Integrating  $d\Phi/B_z = 2\pi r dr$  over radius, we obtain

$$\pi R_0^2 = \int_0^{\Phi_0} \frac{d\Phi}{B_z} = \frac{\Phi_0}{B_{\text{int}}} \int_0^1 \left( 1 + \frac{1}{2} \beta x^2 \right) dx = \frac{\Phi_0}{B_{\text{int}}} \left( 1 + \frac{1}{6} \beta \right), \quad (\text{A7})$$

which yields  $B_{\text{int}} = B_0(1 + \beta/6)$ , where  $B_0 \equiv \Phi_0/(\pi R_0^2)$  is the average field at the upper boundary. Inserting equation (A6) into the expression for the total pressure, we obtain

$$p(\Phi, z_t) = p_{\text{int}}(z_t) + \frac{B_{\text{int}}^2}{8\pi} f(\Phi), \quad (\text{A8})$$

where

$$f(\Phi) \equiv 1 - \left[ 1 + \frac{1}{2} \beta \left( 1 - \frac{\Phi}{\Phi_0} \right)^2 \right]^{-2}. \quad (\text{A9})$$

Comparison of equations (A3) and (A8) shows that  $\Delta p/f(0) = B_{\text{int}}^2/(8\pi)$ , where  $\Delta p \equiv p_{\text{axis}}(z_t) - p_{\text{int}}(z_t)$  is the pressure difference between models C and A at the upper boundary of the cylinder. Inserting the expression for  $B_{\text{int}}$  from equation (A7) yields an equation for  $\beta$ :

$$\left( 1 + \frac{1}{6} \beta \right)^2 \left[ 1 - \left( 1 + \frac{1}{2} \beta \right)^{-2} \right] = \frac{8\pi \Delta p}{B_0^2}, \quad (\text{A10})$$

which is solved by iteration. We find that in the present model  $B_0 = 1.59$  G and  $\beta = 3.78$ , i.e., gas pressure difference produces a significant variation of magnetic field strength across the upper boundary of the flux tube model.

#### REFERENCES

- Avrett, E. H., 1995, in Proc. 15th NSO Sac Peak Workshop, Infrared Tools for Solar Astrophysics: What's Next?, ed. J. Kuhn & M. Penn (Singapore: World Scientific), 303
- Carlsson, M., Judge, P. G., & Wilhelm, K. 1997, ApJ, 486, L63
- Carlsson, M., & Stein, R. F. 1995, ApJ, 440, L29
- . 1997, ApJ, 481, 500
- Choudhuri, A. R., Auffret, H., & Priest, E. R. 1993, Sol. Phys., 143, 49
- Choudhuri, A. R., Dikpati, M., & Banerjee, D. 1993, ApJ, 413, 811
- Collins, W. 1989, ApJ, 337, 548
- . 1992, ApJ, 343, 499
- Curdt, W., & Heinzel, P. 1998, ApJ, 503, L95
- Dere, K. P., & Mason, H. E. 1993, Sol. Phys., 144, 217
- Fontenla, J. M., Avrett, E. H., & Loeser, R. 1990, ApJ, 355, 700
- . 1991, ApJ, 377, 712
- . 1993, ApJ, 406, 319
- Grossmann-Doerth, U., Kneer, F., & von Ueskill, M. 1974, Sol. Phys., 37, 85
- Hansteen, V. H., Betta, R., & Carlsson, M. 2000, A&A, 360, 742
- Hasan, S. S., & Kalkofen, W. 1999, ApJ, 519, 899 (Paper I)
- Hasan, S. S., Kalkofen, W., & van Ballegoijen, A. A. 2000, ApJ, 535, L67
- Heinzel, P., & Curdt, W. 1999, in ASP Conf. Ser. 184, Third Advances in Solar Physics Euroconference: Magnetic Fields and Oscillations, ed. B. Schmieder, A. Hofmann, & J. Staude (San Francisco: ASP), 201
- Hollweg, J. V., Jackson, S., & Galloway, D. 1982, Sol. Phys., 75, 35
- Huang, P., Musielak, Z. E., & Ulmschneider, P. 1995, A&A, 297, 579
- Judge, P., Carlsson, M., & Wilhelm, K. 1997, ApJ, 490, L195
- Judge, P., Tarbell, T. D., & Wilhelm, K. 2001, ApJ, 554, 424
- Kalkofen, W. 1997, ApJ, 486, L148
- Kulsrud, R. M. 1955, ApJ, 121, 461
- Krijger, J. M., Rutten, R. J., Lites, B. W., Straus, Th., Shine, R. A., & Tarbell, T. D. 2001, A&A, 379, 1052
- Lighthill, M. J. 1952, Proc. Roy. Soc. London, A211, 564
- Lites, B. W., Rutten, R. J., & Kalkofen, W. 1993, ApJ, 414, 345
- McAteer, R. T. J., Gallagher, P. T., Williams, D. R., Mathioudakis, M., Phillips, K. J. H., & Keenan, F. P. 2002, ApJ, 567, L168
- McIntosh, S. W., et al. 2001, ApJ, 548, L237
- Muller, R. 1985, Sol. Phys., 85, 113
- Muller, R., Roudier, Th., Vigneau, J., & Auffret, H. 1994, A&A, 283, 232
- Musielak, Z. E., & Rosner, R. 1987, ApJ, 315, 371
- Musielak, Z. E., Rosner, R., Gail, H. P., & Ulmschneider, P. 1995, ApJ, 448, 865
- Musielak, Z. E., Rosner, R., & Ulmschneider, P. 1989, ApJ, 337, 470
- Osterbrock, D. E. 1961, ApJ, 134, 347
- Peter, H. 2001, A&A, 374, 1108
- Press, W. H., Teukolsky, S. A., Vetterling, W. T., & Flannery, B. P. 1992, Numerical Recipes in Fortran (Cambridge: Cambridge Univ. Press), 413
- Roberts, B., & Ulmschneider, P. 1997, Lecture Notes in Phys., 489, 75
- Rosenthal, C. S., et al. 2002, ApJ, 564, 508
- Rutten, R. J., de Pontieu, B., & Lites, B. W. 1999, in ASP Conf. Ser. 183, High Resolution Solar Physics: Theory, Observations, and Techniques, ed. T. R. Rimmele, K. S. Balasubramaniam, & R. R. Radick (San Francisco: ASP), 383
- Spruit, H. C. 1982, Sol. Phys., 75, 3
- Stein, R. F. 1967, Sol. Phys., 2, 385
- . 1968, ApJ, 154, 297

- Steiner, O., Grossmann-Doerth, U., Knölker, M., & Schüssler, M. 1998, ApJ, 495, 468
- Ulmschneider, P., Kalkofen, W., Nowak, T., & Bohn, H. U. 1977, A&A, 64, 61
- Ulmschneider, P., & Musielak, Z. E. 1998, A&A, 338, 311
- Ulmschneider, P., Zähringer, K., & Musielak, Z. E. 1991, A&A, 241, 625
- van Ballegoijen, A., Nisenson, P., Noyes, R. W., Löfdahl, M. G., Stein, R. F., Nordlund, A., Krishnakumar, V. 1998, ApJ, 509, 435
- Vernazza, J. E., Avrett, E. H., & Loeser, P. 1981, ApJS, 45, 635
- von Uexküll, M., & Kneer, F. 1995, A&A, 294, 252
- Wikstøl, Ø., Hansteen, V. H., Carlsson, M., & Judge, P. G. 2000, ApJ, 531, 1150
- Zhugzhda, Y. D., Bromm, V., & Ulmschneider, P. 1995, A&A, 300, 302 579